Quasi-Static and Impact Response of Graded Aluminium Matrix Syntactic Foams

Chen Liang[a *] and Yuyuan Zhao[b]

School of Engineering, University of Liverpool, Liverpool L69 3GH, UK

[a]liangc@liverpool.ac.uk, [b]yyzhao@liverpool.ac.uk

Keywords: syntactic foam, graded structure, compression, impact, energy absorption.

Abstract. The behaviour of aluminium matrix syntactic foams (AMSFs) with homogeneous and graded structures have been studied under quasi-static compression and impact. Particle size of ceramic microspheres and impact velocity had significant effects on the static and impact responses. Smaller microspheres led to higher strength but lower toughness. The compressive yield stress, plateau stress and specific energy absorption of the graded AMSF specimens were approximately the averages of the constituent layers, following the rule of mixture, although the order of the layers had some influence on the compressive behaviour. The syntactic foams were brittle under impact, no matter whether they were brittle or ductile in quasi-static compression. They had higher peak stresses and absorbed more energy in impact than in quasi-static compression. The location of the most brittle layer of the small ceramic microspheres had a significant effect on the impact failure pattern and sequence of the three-layer graded AMSFs.

Introduction

Aluminum matrix syntactic foams (AMSFs) are a novel class of lightweight materials, where hollow ceramic particles such as alumina cenospheres [1,2] and fly ash [3,4] are embedded in an aluminium alloy matrix. AMDFs offer advantages of low weight, high specific stiffness, improved strength and high damage tolerance due to mechanical energy absorption capabilities. These properties make syntactic foams suitable for many applications such as cores in sandwich structures, crash protection and damping panels [5]. Syntactic foams can be designed to meet different application demands by selecting appropriate hollow spheres [6].

The majority of AMSFs studied up to date are manufactured by melt infiltration casting and have homogeneous structures [7]. A large amount of research has been conducted to investigate their mechanical properties, including compressive response and energy absorption capacity [8], failure mechanisms [9] and impact response [10,11]. Several attempts have been made to improve the mechanical properties of AMSFs using bimodal ceramic microspheres [12] or introducing Al particles [13].

Graded syntactic foams with different volume fractions or particle sizes of ceramic have been fabricated to improve energy absorption under compression [14]. In order to tailor the physical and mechanical properties of graded syntactic foams, separate layers with gradient in volume fraction and wall thickness of microballoons have been bonded with an adhesive like epoxy [15]. However, syntactic foams fabricated by this approach have poor structural integrity between layers, which in turn has a detrimental effect on the mechanical properties of the syntactic foams.

In this study, AMSFs with graded structures consisting of integral two or three layers of ceramic microspheres with different particle sizes have been fabricated by infiltration casting in one operation. Quasi-static compression and dynamic impact tests have been conducted to study the compressive and impact responses and energy absorption capabilities of homogeneous and graded AMSFs. The effects of layer type and order of the graded AMSFs on the pattern and sequence of compressive and impact failures have been investigated.

Experimental

The AMSF samples were produced by infiltration casting [8] using a 6082 Al alloy and the hollow ceramic microsphere (CM) powder supplied by Envirospheres Pty Ltd. The CM powder has a composition of ~60% SiO_2, ~40% Al_2O_3 and 0.4-0.5% Fe_2O_3 by weight and was separated into three powders with particle size ranges of 75-150 μm, 125-250 μm and 250-500 μm, designated as small (S), medium (M) and large (L), respectively. The three CM powders have a similar density of 0.66 g/cm^3. Before infiltration, a steel tube, sealed by a circular steel disc at bottom, was filled either with one layer of the same CM powder or with two or three layers of different CM powders. An Al alloy block was then placed on top of the CM powder(s) and another circular steel disc was placed above the Al block. The assembly was heated to 785°C for 30 minutes in an electric furnace before being moved to a hydraulic machine where the molten Al alloy was compressed into the voids between the CM particles. After solidification, the resultant AMSF sample was removed from the steel tube and ground into cuboid specimens with dimensions of 15×15×15 mm for quasi-static compression tests and 10×10×15 mm for impact tests. The homogeneous AMSF specimens are designated as L, M and S, while the two-layer graded specimens as LM, LS and MS, and the three-layer graded specimens as LMS, MLS and LSM. The letters represent the type and sequence of the CM powders contained in the specimens. The layer thickness is 15 mm, 7.5 mm and 5 mm for one-, two- and three-layer specimens, giving a total specimen thickness of 15 mm. All the AMSF specimens have a density approximately 1.55 g/cm^3, containing 55% CM particles. Optical micrographs of the typical AMSF specimens are shown in Fig. 1.

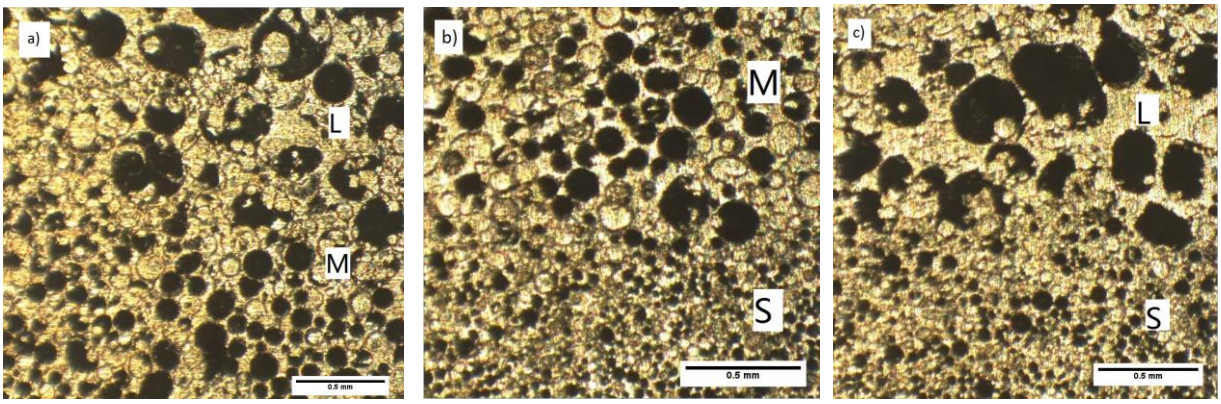

Fig. 1 Optical micrographs of graded AMSFs showing interfacial regions between layers containing a) large and medium, b) medium and small, and c) large and small CM powders.

Results and Discussion

Quasi-static compression. The compressive stress-strain curves of the AMSFs are presented in Fig. 2. The curves have the same general characteristics as the other AMSFs [16,17]. There is a linear portion indicating elasticity and then a drop in stress corresponding to the onset of crushing of the CMs. An extended plateau stress follows while porosity is decreasing, before the stress finally increases at the completion of densification. Table 2 shows the densification strain, yield stress, plateau stress and specific energy absorption for these specimens obtained from the stress-strain curves. The specific energy absorption is the energy absorbed up to densification by per unit mass of AMSF and is calculated as the area under the compressive stress-strain curve up to the densification strain divided by the density of the AMSF specimen.

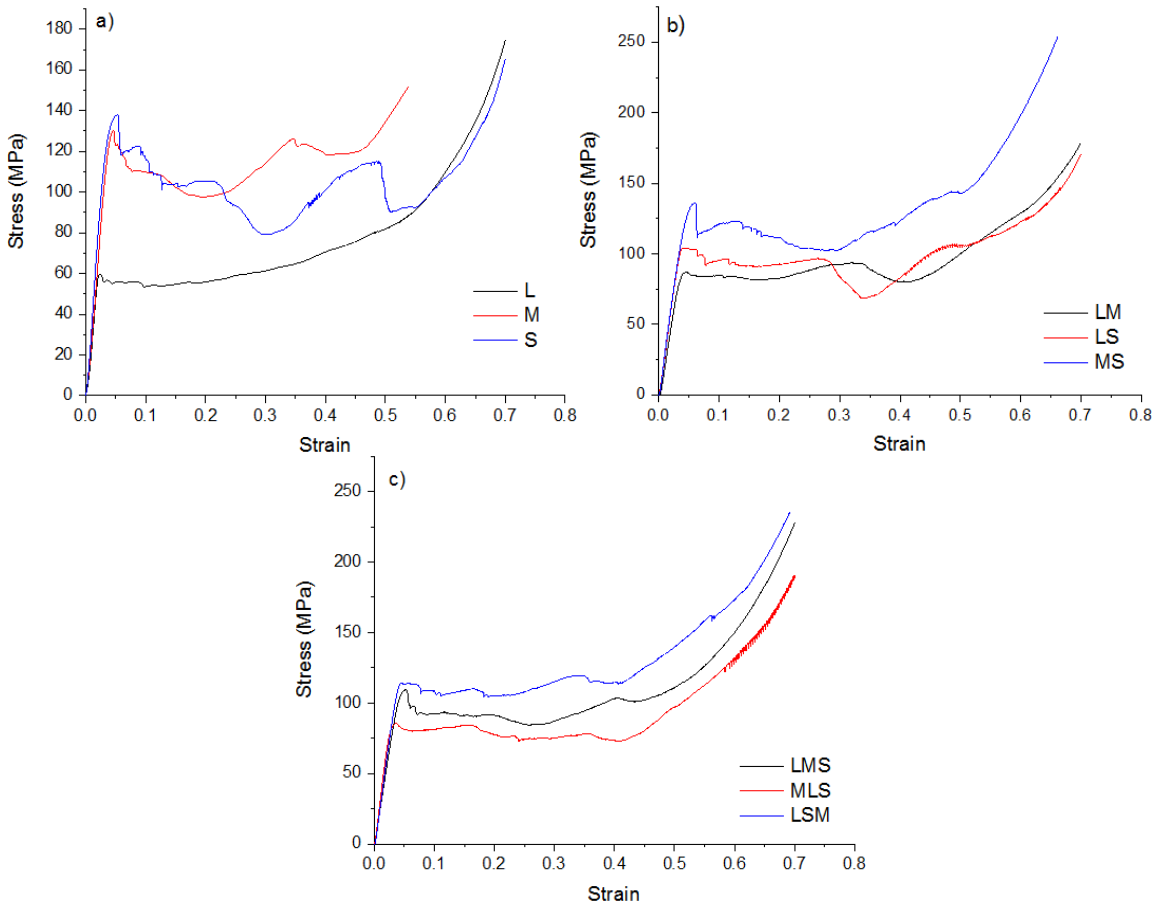

Fig. 2 Quasi-static compression stress-strain curves of a) homogeneous, b) two-layer and c) three-layer AMSFs.

Table 1 Quasi-static compressive properties of AMSFs

	Densification strain	Yield stress (MPa)		Plateau stress (MPa)		Specific energy absorption (J/g)	
		Measured	ROM	Measured	ROM	Measured	ROM
L	0.45	59.8		55.9		20.3	
M	0.49	130.1		114.1		31.5	
S	0.50	137.8		105.4		32.1	
LM	0.48	86.8	94.5	84.5	85	24.6	25.9
MS	0.51	135.9	133.9	112.8	109.8	32.7	31.8
LS	0.52	103.9	98.8	93.9	80.7	26.8	26.2
LMS	0.49	109.3	109.2	92.5	91.8	28.2	28.0
MLS	0.47	85.9	109.2	77.9	91.8	22.4	28.0
LSM	0.43	114.0	109.2	108.2	91.8	28.4	28.0

Fig. 2 (a) shows that the homogenous specimens L, M and S have different yield stresses of 59.8, 130.1 and 137.8 MPa and plateau stresses of 55.9, 114.1 and 105.4 MPa, respectively. Specimen L is ductile and has no significant stress decline at the onset of CM crushing, while specimens M and S are brittle and show significant stress declines in the plateau region.

The yield stress, plateau stress and specific energy absorption of the graded AMSF specimens in Fig. 2(b) and (c) are approximately the averages of the constituent layers, i.e., roughly following the rule of mixture (ROM) as shown in Table 2. However, the order of the layers has some influence on the compressive behaviour. The yield stress and plateau stress of the three-layer AMSF specimens vary with the order of layers, affected more by the middle layer. In other words, the middle layer in the three-layer specimens has more contribution to the yield stress and plateau stress.

An interesting observation of the graded AMSFs is that they have a single yield point and a single plateau region. This behavior is different from that observed in a simple overlay of two homogeneous specimens. Fig. 3 compares a graded AMSF specimen with a simple overlay of two homogeneous AMSF specimens. Fig. 3(a) shows that the weaker layer (L) yields first and is completely crushed before the stronger layer (S) starts to yield. This two-stage deformation is evidenced in the compressive stress-strain curve (Fig. 4), where two yield points and two plateau stresses are present. It can also be seen that there is obviously horizontal slide between the two homogeneous specimens during compression. This phenomenon of interfacial slide was also observed in foams glued together by epoxy [15]. In the graded AMSFs, there is a coordinated deformation in the layers. It seems the integral interlayer boundaries promote the structural integrity of the graded AMSFs and therefore prevent the sequential layer-by-layer deformation.

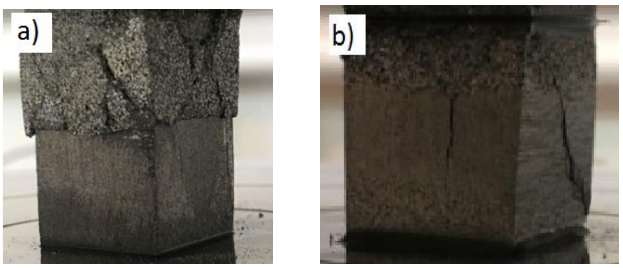

Fig. 3 Deformation of a) a simple overlay of homogeneous AMSFs and b) a graded AMSF under quasi-static compression

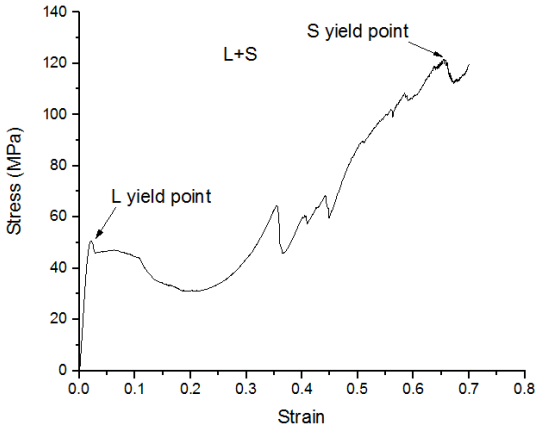

Fig. 4 Quasi-static compression stress-strain curves of an overlay of two homogeneous AMSFs (L and S)

Impact. Fig. 5 shows typical variations of hammer velocity as a function of strain recorded by the high-speed camera, using the graded LSM specimen as an example. These curves were used to calculate the energy absorption as a function of strain, which will be presented and discussed later.

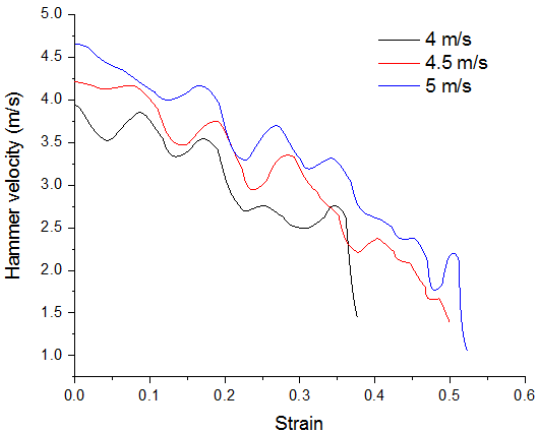

Fig. 5 Hammer velocity as a function of strain for the graded AMSF LSM under impact loading

The stress-strain curves for the homogeneous and graded AMSFs under impact loading at different impact velocities are shown in Fig. 6. Only the first impact before the stress drops to zero is considered here. It can be seen that the peak stress (shown in Table 2) experienced in impact is significantly higher than that in quasi-static compression for all specimens. The impact stress-strain curve sometimes changes significantly when the impact is varied. However, the high peak stresses (>200 MPa) are associated with specimens that have a strong and brittle outside S layer. Specimens that do not contain an S layer, or contain an S layer sandwiched between more ductile L and M layers, have moderate peak stresses.

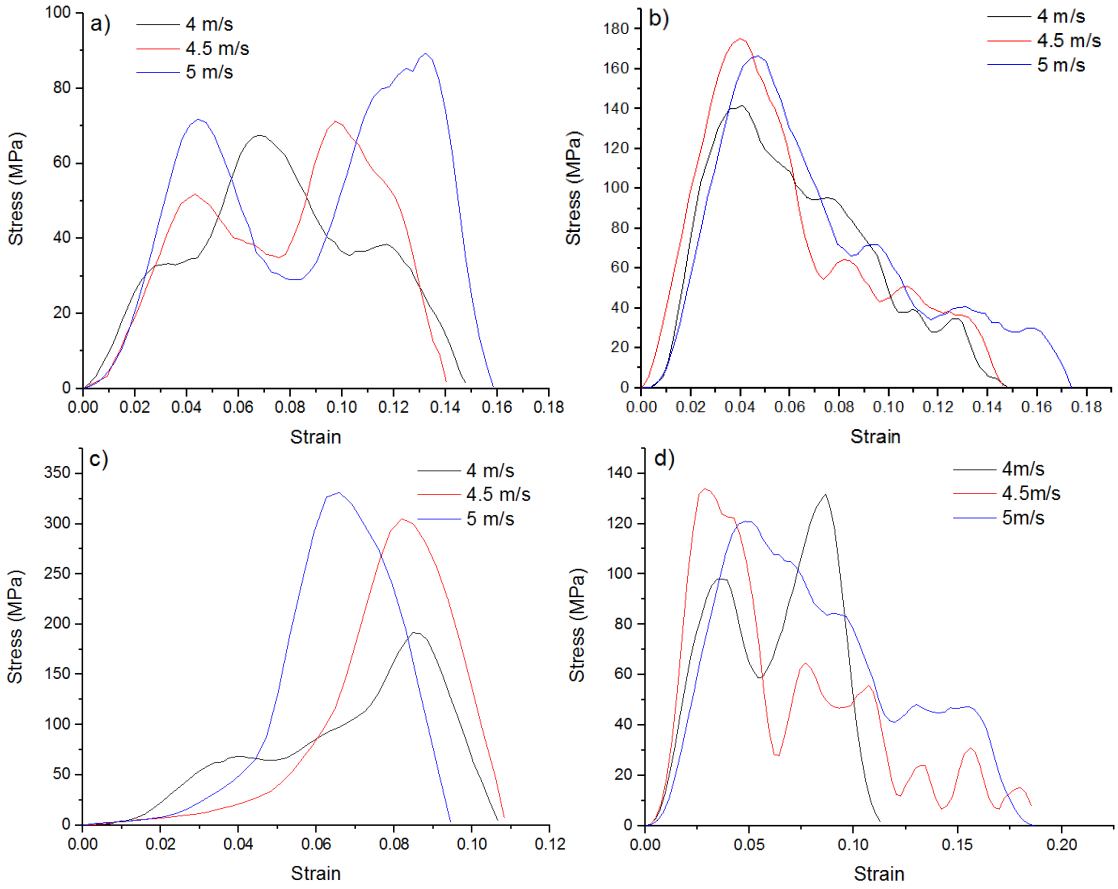

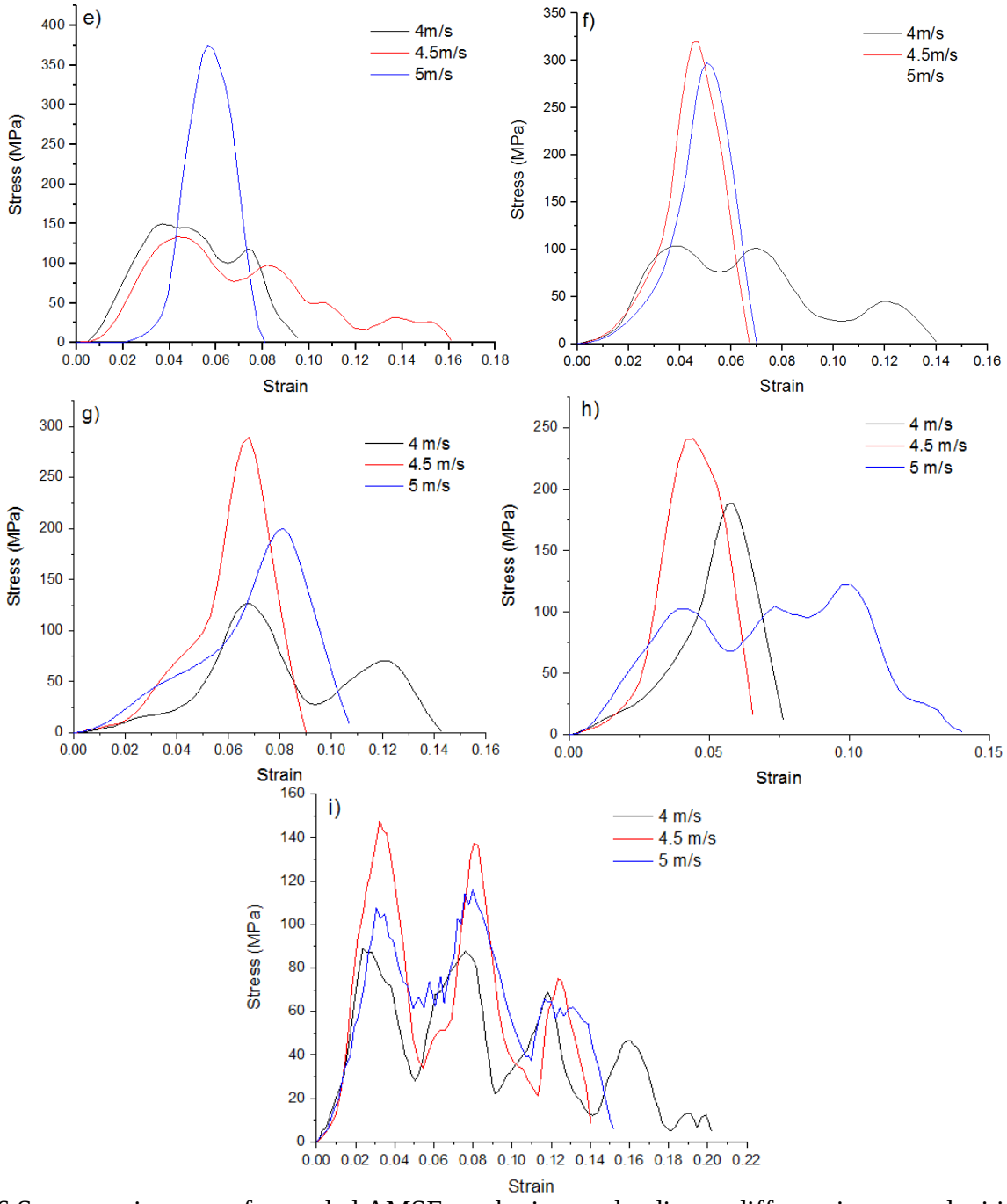

Fig. 6 Stress-strain curves for graded AMSFs under impact loading at different impact velocities: a) L, b) M, c) S, d) LM, e) MS, f) LS, g) LMS, h) MLS, and i) LSM

Table 2 Peak stress of AMSFs under impact loading at different impact velocities

	Peak stress (MPa)		
	4m/s	4.5m/s	5m/s
L	67.5	71.2	89.4
M	141.9	175.4	166.5
S	191.8	305.2	331.4
LM	131.8	133.9	121.0
MS	150.1	134.1	375.6
LS	103.4	320.0	297.7
LMS	126.7	289.3	199.8
MLS	188.6	241.1	122.5
LSM	89.2	147.7	115.8

Failure patterns. Table 3 lists the failure patterns of the homogeneous and graded AMSF specimens observed during impact. We examined the impact video images recorded by the high speed camera frame by frame to observe the sequence of failure under impact. Fig. 7 shows representative failure patterns present in the images. It should be noted that, due to the relatively long time interval between the frames (0.2 ms), it is difficult to capture all the representative images of the first impact, which lasts for only about 0.5 ms.

Table 3 Failure sequence of AMSFs under impact at different impact velocities

	4 m/s	4.5 m/s	5 m/s
L	crush	crush →crack	crush →crack
M	crush→crack	crack→crush	x.crack
S	crack	crack→x.crack	x.crack
LM	int.crack→crack in L →crush in M	crack in L→int.crack →crush in M	x.crack
MS	crush in M→x.crack in S	crack	x.crack
LS	int.crack → crack in L → crack in S	crush in L→crack in S	int.crack →crush in L →crack in S
LMS	crack	crack in S→x.crack	x.crack
MLS	crack in L→crush in M →crack in S	int.crack in LS→x.crack in LM→ crack in S	int.crack in LM and LS →crush
LSM	crush in L→x.crack in S →crush in M	crush in L→x.crack in S →crush in M	crush in L→x.crack S →crush in M

Note: crack – single crack; x.crack- x-shaped crack; int.crack- interfacial crack

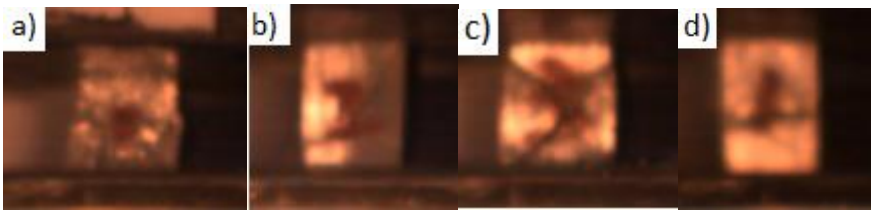

Fig. 7 Representative failure patterns in AMSFs under impact: a) crush, b) single crack, (c) x-shaped crack, (d) interfacial crack

Several failure patterns can be observed in specimens during impact, including crush, single crack, x-shaped crack and interfacial crack (i.e., horizontal crack at the interface between two layers). Crush is a progressive collapse process that happens in more ductile L and sometimes in less ductile M layers, while cracks can form in L, M and S layers. The S layers always fail by brittle fracture. The failure pattern and sequence in the AMSFs are complex, but a few observations can be made. Firstly, increasing impact velocity tends to increase the occurrence of brittle fracture, i.e., from ductile crush to brittle crack or from single crack to more brittle x-shaped crack. Secondly, interfacial cracks are observed at the interfaces between L and M, and between L and S, but not observed at the interfaces between M and S. It seems the strength of the interfacial region between two layers is dependent on the particle size difference, which is very large between L and S (with a difference in mean particle size of 262.5 μm), large between L and M (187.5 μm), and relatively small between M and S (75 μm). In other words, the interfacial region between two similar layers is stronger than between two very dissimilar layers. Thirdly, the location of the brittle S layer in the graded AMSFs has a significant influence on the failure pattern. When the S layer is situated in the middle (LSM), the specimen fails by layer by layer fashion with crush in the L and M layers and fracture in the S layer, associated with relatively low peak stress as shown in Table 2. High peak

stresses in Table 2 appear in specimens that have an outside S layer, which fail by fracture across the whole specimen, often associated with x-shaped cracks.

Energy absorption. Fig. 8 shows the specific energy absorption as a function of strain for the homogeneous and graded AMSF specimens under quasi-static compression and impact. For quasi-static compression, the energy absorption was obtained by integrating the stress-strain curve. For impact, the energy absorption was considered as the kinetic energy loss of the hammer, which was obtained from the hammer velocity recorded by the high speed camera (Fig. 5).

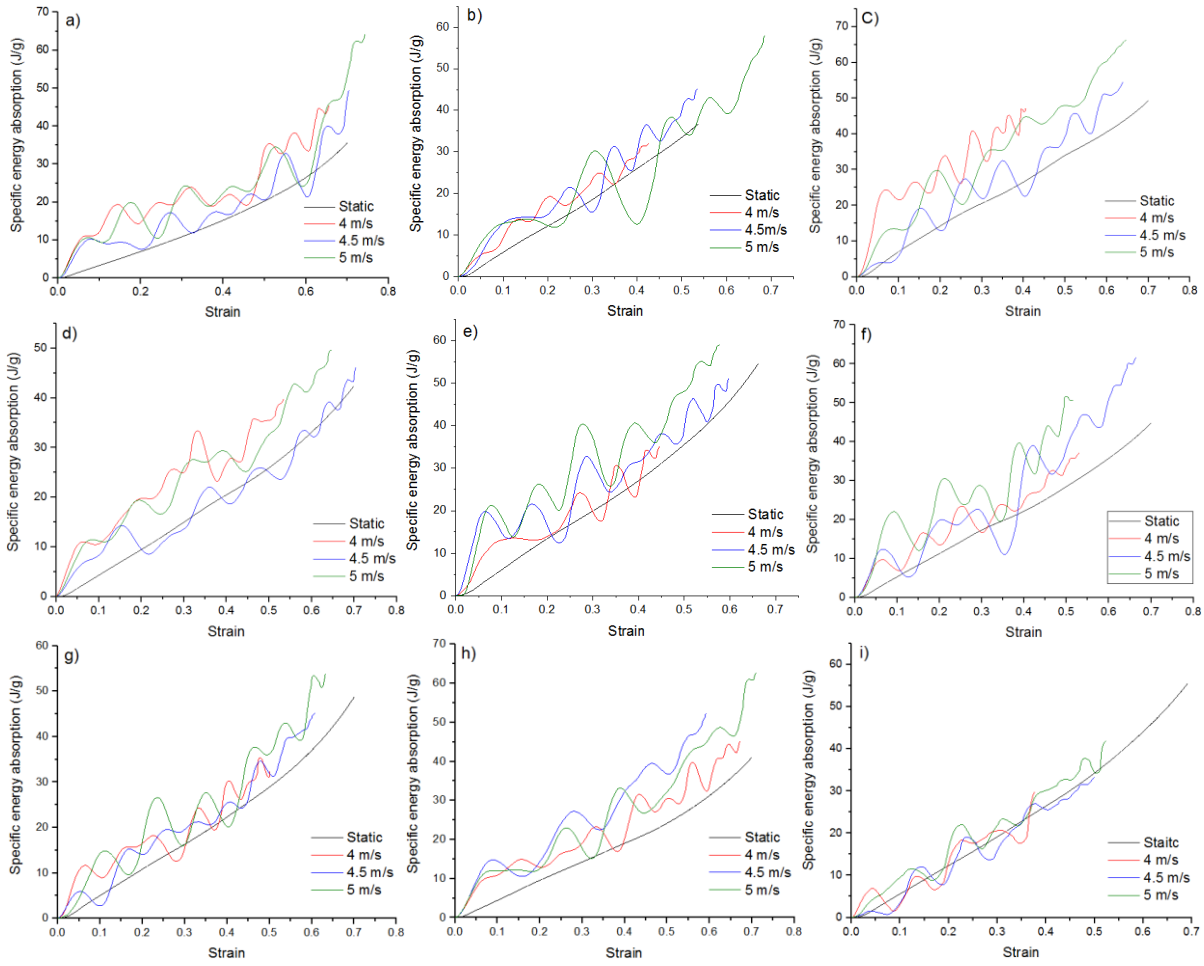

Fig. 8 Specific energy absorption as a function of strain for AMSFs: a) L, b) M, c) S, d) LM, e) MS, f) LS, g) LMS, h) MLS, i) LSM

All the AMSF specimens, except LSM, absorb more energy in impact than in quasi-static compression, as shown in Fig. 8, while the effect of impact velocity is not significant. The impact energy absorption curves show two distinctive stages. There is a sharp increase in energy absorption before the strain reaches 0.1, which corresponds to the end of the first impact. The energy absorption increases steadily with increasing strain above 0.1, with the same slope as the quasi-static compressive curve. It indicates that first impact absorbs significantly more energy than quasi-static compression due to higher peak stress in impact loading than in quasi-static compression. After the first impact, the energy absorption behavior in impact is similar to that in quasi-static compression.

The specimen LSM shows a different pattern. The first impact absorbs similar amount of energy as in quasi-static compression, because both loading conditions result in a similar peak stress. After first impact, the impact energy absorption is similar to quasi-static compression as in other specimens. As a consequence, the impact energy absorption curve follows the same trend as the

compressive energy absorption curve throughout the whole strain range. This also confirms that first impact is the cause for the higher energy absorption in impact than in quasi-static compression.

Conclusions

1. The compressive yield stress, plateau stress and specific energy absorption of the graded AMSF specimens generally followed the rule of mixture. They were approximately the averages of the constituent layers. The order of the layers had some influence on the compressive behavior.
2. The AMSFs were brittle under impact and had higher peak stresses and absorbed more energy than in quasi-static compression. The location of the brittle S layer in the graded AMSFs had a significant influence on the failure pattern. The graded AMSF with the S layer in the middle failed by a layer-by-layer fashion and showed a relatively low peak stress, while high peak stresses were associated with specimens with an outside S layer.
3. The AMSFs absorbed more energy in impact than in quasi-static compression, due to higher peak stress in first impact. After the first impact, the energy absorption behavior is similar in both impact and quasi-static compression.

Acknowledgements

Liang would like to thank the China Scholarship Council and the University of Liverpool for a PhD studentship (Grant No.201608340070).

References

[1] M.Y. He, F.W. Zok, M. Kiser, The mechanical response of ceramic microballoon reinforced aluminum matrix composites under compressive loading, Acta Mater. 47 (1999) 2685-2694.

[2] M. Alizadeh, M. Mirzaei-Aliabadi, Compressive properties and energy absorption behavior of AleAl2O3 composite foam synthesized by space-holder technique, Mater. Des. 35 (2012) 419-424.

[3] P.K. Rohatgi, J.K. Kim, R.Q. Guo, et al. Age-hardening characteristics of aluminum alloy-hollow fly ash composites, Metall. Mater. Trans. A 33 (2002) 1541-1547.

[4] P.K. Rohatgi, A. Daoud, B.F. Schultz, et al. Microstructure and mechanical behaviour of die casting AZ91D-fly ash cenosphere composites, Compos. Part A. 40 (2009) 883-896.

[5] M.D. Goel, V.A. Matsagar, A.K. Gupta, Blast resistance of stiffened sandwich panels with aluminum cenosphere syntactic foam, Int. J. Impact Eng. 77 (2015) 134-146.

[6] Y.F. Lin, Q. Zhang, G.H. Wu, Interfacial microstructure and compressive properties of Al-Mg syntactic foam reinforced with glass cenospheres, J. Alloys and Compounds. 655 (2016) 301-308.

[7] Y.Y. Zhao. Metal matrix syntactic foams: manufacture, matrix material, microstructure, modulus and more, JOM. 63 (2011) 35.

[8] L.P. Zhang, Y.Y. Zhao. Mechanical response of Al matrix syntactic foams produced by pressure infiltration casting, J. Composite Mater. 41 (2007) 2105-2117.

[9] X.F. Tao, Y.Y. Zhao. Compressive failure of Al alloy matrix syntactic foams manufactured by melt infiltration, Mater. Sci. Eng. A. 549 (2012) 228-232.

[10] M. Altenaiji, Z.W. Guan, W.J. Cantwell et al. Characterisation of aluminium matrix syntactic foams under drop weight impact, Mater. Design. 59 (2014) 296-302.

[11] M. Altenaiji, G. Zhongwei, W. Cantwell, et al. Characterisation of aluminium matrix syntactic foams dynamic loading, Adv. Mech. Manuf. Eng. 564 (2014) 449-454.

[12] X.F. Tao, L.P. Zhang, Y.Y. Zhao. Al matrix syntactic foam fabricated with bimodal ceramic microspheres, Mater. Design. 30 (2009) 2732-2736.

[13] X.F. Tao, Y.Y.Zhao. Compressive behavior of Al matrix syntactic foams toughened with Al particles, Scripta Mater. 61 (2009) 461-464.

[14] Kishore, R. Shankar, S. Sankaran. Gradient syntactic foams: Tensile strength, modulus and fractographic features, Mater. Sci. Eng. A. 412 (2005) 153-158.

[15] N. Gupta, W. Ricci. Comparison of compressive properties of layered syntactic foams having gradient in microballoon volume fraction and wall thickness, Mater. Sci. Eng. A. 427 (2006) 331-342.

[16] D.K. Balch, J.G. O'Dwyer, G.R. Davis, et al. Plasticity and damage in aluminum syntactic foams deformed under dynamic and quasistatic conditions, Mater. Sci. Eng A. 391 (2005) 408e17.

[17] N. Gupta, E. Woldesenbet, P. Mensah. Compression properties of syntactic foams: effect of cenosphere radius ratio and specimen aspect ratio, Composites Part A. 35 (2004) 103e11.